

Strong electron-phonon coupling in $\text{Ba}_{1-x}\text{Sr}_x\text{Ni}_2\text{As}_2$

Linxing Song,^{1,2} Jianguo Si,³ Tom Fennell,⁴ Uwe Stuhr,⁴ Guochu Deng,⁵ Jinchen Wang,⁶ Juanjuan Liu,⁶ Lijie Hao,⁷ Huiqian Luo,^{1,3} Miao Liu,^{1,8,3} Sheng Meng,^{1,2,3,*} and Shiliang Li^{1,2,3,†}

¹*Beijing National Laboratory for Condensed Matter Physics,
Institute of Physics, Chinese Academy of Sciences, Beijing 100190, China*

²*School of Physical Sciences, University of Chinese Academy of Sciences, Beijing 100190, China*

³*Songshan Lake Materials Laboratory, Dongguan, Guangdong 523808, China*

⁴*Laboratory for Neutron Scattering and Imaging,
Paul Scherrer Institute, CH-5232 Villigen-PSI, Switzerland*

⁵*Australian Centre for Neutron Scattering, Australian Nuclear Science
and Technology Organisation, Lucas Heights, NSW 2234, Australia*

⁶*Laboratory for Neutron Scattering and Beijing Key Laboratory
of Optoelectronic Functional Materials and MicroNano Devices,*

Department of Physics, Renmin University of China, Beijing 100872, China

⁷*China Institute of Atomic Energy, PO Box 275-30, Beijing 102413, China*

⁸*Center of Materials Science and Optoelectronics Engineering,
University of Chinese Academy of Sciences, Beijing 100049, China*

The charge density wave (CDW) or nematicity has been found to coexist with superconductivity in many systems. Thus, it is interesting that the superconducting transition temperature T_c in the doped BaNi_2As_2 system can be enhanced up to six times as the CDW or nematicity in the undoped compound is suppressed. Here we show that the transverse acoustic phonons of $\text{Ba}_{1-x}\text{Sr}_x\text{Ni}_2\text{As}_2$ are strongly damped in a wide doping range and over the whole Q range, which excludes its origin from either CDW or nematicity. The damping of TA phonons can be understood as large electron-phonon coupling and possible strong hybridization between acoustic and optical phonons as shown by the first-principle calculations. The superconductivity can be quantitatively reproduced by the change of the electron-phonon coupling constant calculated by the McMillan equation in the BCS framework, which suggests that no quantum fluctuations of any order is needed to promote the superconductivity. On the contrary, the change of T_c in this system should be understood as the sixfold suppression of superconductivity in undoped compounds.

I. INTRODUCTION

The electronic nematic phase breaks the rotational symmetry of the underlying lattice and in theory, its quantum fluctuations may enhance superconductivity [1–5]. Experimentally, nematicity has been widely found in cuprates and iron-based superconductors, where nematic quantum fluctuations have been suggested to play important roles in promoting superconductivity [6–19]. In the mean time, doubts on the effects of nematic fluctuations on superconductivity have also been raised [20–23]. One of the major obstacles in further investigating the relationship between the nematicity and superconductivity in both systems is the existence of the antiferromagnetic (AFM) order and its strong fluctuations [24–28]. It has been shown recently that the $\text{Ba}_{1-x}\text{Sr}_x\text{Ni}_2\text{As}_2$ (BSNA) system may offer an opportunity to study the role of nematic fluctuations on superconductivity without the influence from AFM fluctuations [29].

The structures of both BaNi_2As_2 and SrNi_2As_2 are ThCr_2Si_2 type at room temperature [30–32]. The former changes to the triclinic structure at $T_s = 135$ K [30, 31, 33], while the latter stays in the tetragonal structure down to the lowest temperature. Interestingly, both

of them show superconductivity at similar temperatures between 0.6 and 0.7 K despite their structural difference at low temperatures [30–32]. Moreover, both of them show no magnetism, which suggests that the superconducting mechanism may be associated with conventional phonon-mediated pairing [34]. The structure transition in BaNi_2As_2 can be suppressed by chemical doping, such as phosphorus, copper, cobalt, and strontium, and the T_c shows up to sixfold enhancement near the structural instability [29, 35–38]. Such a phenomenon has also been observed in other nickel pnictides [39, 40], suggesting a general mechanism to enhance superconductivity.

The enhancement of superconductivity in doped BaNi_2As_2 systems may be associated with the quantum fluctuations of two phases. The first one is nematicity, which has been suggested to exist in both BSNA and $\text{BaNi}_2(\text{As,P})_2$ systems [29, 41, 42]. The nematic transition temperature extracted from the Curie-Weiss-like fitting of the elastoresistivity becomes zero near optimal doping, which resembles the case in iron-based superconductors [7, 10–12]. The second phase involved is the charge density wave (CDW). Two types of CDWs have been found in BaNi_2As_2 , an incommensurate CDW (IC-CDW) above T_s and a commensurate CDW (C-CDW-1) below it [43]. In BSNA, a new commensurate CDW (C-CDW-2) appears above $x = 0.4$ [44], as shown in Fig. 1(a). The appearance and enhancement of superconductivity near the CDW instability have been widely found

* smeng@iphy.ac.cn

† slli@iphy.ac.cn

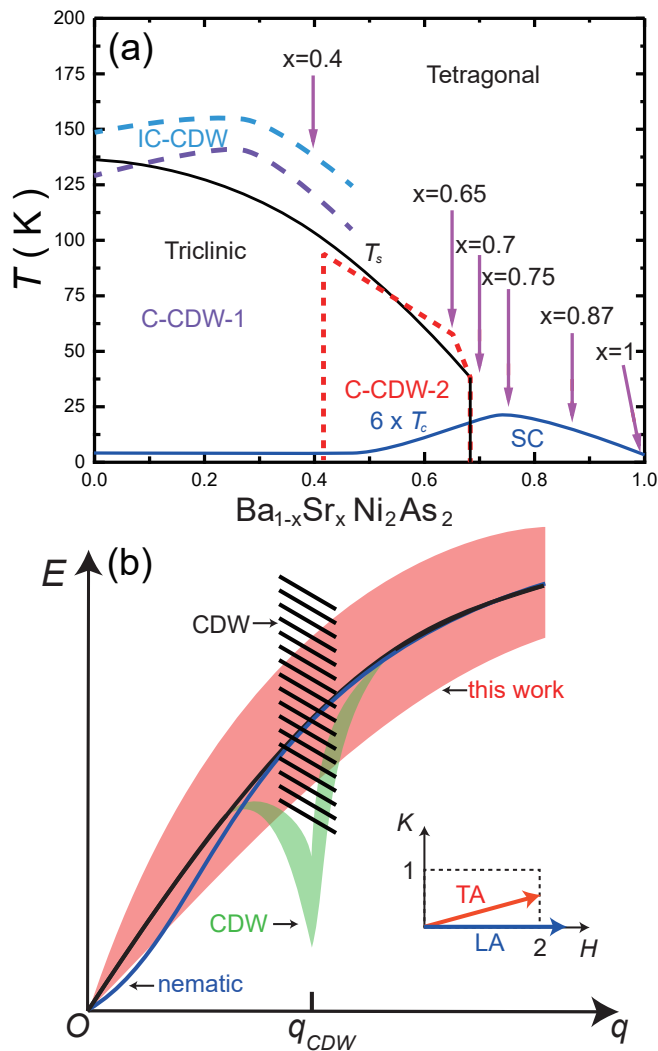


FIG. 1. (a) Schematic phase diagram of $\text{Ba}_{1-x}\text{Sr}_x\text{Ni}_2\text{As}_2$ based on the data in Refs. [29, 44]. SC stands for superconductivity. The arrows indicate the samples measured by INS in this work. (b) Schematic effects of nematic fluctuations and CDW on the acoustic phonons. The black and blue lines are unaffected phonon dispersion and that under nematic fluctuations, respectively. The change of phonons by CDW are illustrated by the green shaded area and black oblique lines, respectively. The pink area indicates the results of this work. The inset shows the schematic scans to measure the TA and LA phonons around the $(2,0,0)$.

in many other systems [45–49]. Whether the BSNA system falls into the same category is interesting and unclear. We note that both CDW and nematic order have effects on phonon spectra, as roughly illustrated in 1(b), and thermodynamical measurements have indicated significant phonon softening when the CDW disappears [29, 35, 36, 50]. Thus, it is crucial to further investigate the pairing mechanism by studying the phonons.

In this work, we studied the acoustic phonons in BSNA by the inelastic neutron scattering (INS) tech-

nique. Wide Q -range damping of the transverse acoustic (TA) phonons are found in all samples around the optimal doping. Such large damping of TA phonons can be understood by neither CDW nor nematic fluctuations. By comparing with the first-principle calculations, we show that the superconductivity around the optimal doping level can be well understood by the McMillan equation in the BCS theory without invoking the quantum fluctuations from either CDW or nematicity.

II. EXPERIMENTS

Single crystals of BSNA were grown by the self-flux method as reported previously [29]. The INS experiments were carried out on the thermal triple-axis spectrometers EIGER [51] at SINQ, Switzerland, TAIPAN at ANSTO, Australia [52], and cold neutron multiplexing spectrometer BOYA at CARR, China. The information of all samples is listed in the Supplemental Material [53]. The samples were measured in the $[H, K, 0]$ scattering plane with the momentum transfer $\mathbf{Q} = H\mathbf{a}^* + K\mathbf{b}^* + L\mathbf{c}^*$, where the reciprocal lattice parameters \mathbf{a}^* , \mathbf{b}^* and \mathbf{c}^* are defined in the tetragonal lattice with $a = b \approx 4.144 \text{ \AA}$ and $c \approx 11.633 \text{ \AA}$. The TA and longitudinal acoustic (LA) phonons were measured by scans along $[2, K, 0]$ and $[H, 0, 0]$, respectively, as shown in the inset of Fig. 1(b). The resolutions of the instruments were calculated by the ResLibCal program [54], where the effects of sample mosaics have been included. The first-principles calculations were performed via the QUANTUM ESPRESSO package [55] with the virtual crystal approximation method [56]. The ultrasoft pseudopotentials with the generalized gradient approximation was used to create the pseudopotential of fake atoms, and which is parametrized by the Perdew-Burke-Ernzerhof function [57]. Phonon dispersion curves were calculated based on the density functional perturbation theory [58], where a denser $16 \times 16 \times 16$ ($16 \times 16 \times 12$) k -point grid and a $4 \times 4 \times 4$ ($4 \times 4 \times 3$) q -point grid were employed for the electron-phonon coupling (EPC) calculations of the tetragonal (triclinic) phase.

III. RESULTS AND DISCUSSIONS

Figures 2(a) and 2(b) show constant- Q scans at $[2, K, 0]$ for the TA phonons in the $x = 0.65$ sample at 150 and 5 K, respectively. Since the crystal structure at 5 K is triclinic, the nominal $[2, K, 0]$ in the tetragonal notation approximately corresponds to $[2, K, -1-K/2]$ in the triclinic notation. To quantitatively study the phonon dispersion, we use the following damped harmonic-oscillator function [59] to fit the constant- Q scans,

$$S(Q, E) = \frac{A}{E_c(1 - e^{-E/k_B T})} \frac{\Gamma/2}{(E - E_c)^2 + \Gamma^2/4} \quad (1)$$

where E_c , Γ and A are the phonon energy, the peak full-width at half-maximum (FWHM) and the fitting con-

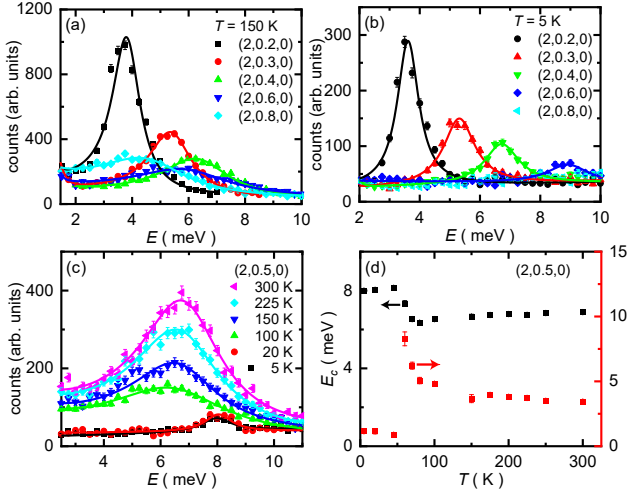


FIG. 2. The results of TA phonons for the $x = 0.65$ sample. (a), (b) Constant- Q scans along $[2, K, 0]$ at 150 and 5 K, respectively. The solid lines are fitted by Eq. (1). (c) Constant- Q scans at $(2, 0.5, 0)$ at various temperatures. The solid lines are fitted by Eq. (1). (d) The temperature dependence of phonon energy and width at $(2, 0.5, 0)$.

stant. The backgrounds are fitted by a constant plus a Gaussian function with the center fixed at zero energy to account for the tail from the elastic incoherent nuclear scattering.

Figure 2(c) shows the constant- Q scans at $(2, 0.5, 0)$ at various temperatures, which is the Q position associated with the C-CDW-2. Figure 2(d) gives the temperature dependence of the corresponding E_c and Γ . The value of E_c only slightly decreases with decreasing temperature when approaching T_s , whereas Γ shows a quick upturn below about 80 K. While such upturn is associated with the CDW transition, the almost temperature-independent large Γ above 100 K should not be. Below the structural or CDW transition, E_c changes because of the triclinic structure at low temperatures and Γ becomes much smaller.

Figures 3(a) and 3(b) show the constant- Q scans at $(2, 0.3, 0)$ and $(2, 0.5, 0)$, respectively, for other samples at 150 K. The data at 5 K of the $x > 0.75$ samples show no significant difference as there is no structural transition [53]. With decreasing x , the peak position decreases while the width becomes broader. The data can all be well fitted by Eq. (1), which gives TA phonon dispersions and FWHMs in Figs. 3(c) and (d), respectively. It is clear that TA phonons become softer with decreased x while the damping effect gets larger in the tetragonal structure (150 K). We note that a minimum appears around $K \approx 0.8$, which may come from the low-energy optical phonons that are strongly coupled with the TA phonons as shown later, considering that the condition for measuring TA phonons by INS is not well satisfied anymore at large K 's. The phonon dispersion of the $x = 0.65$ sample at 5 K is different from that at 150 K,

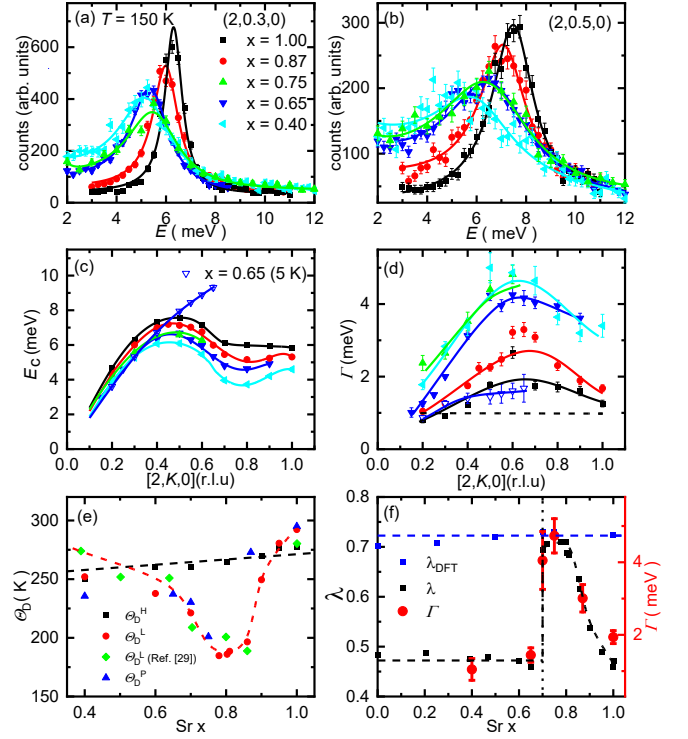


FIG. 3. Summary of the TA phonons in BSNA. (a), (b) Constant- Q scans at $(2, 0.3, 0)$ and $(2, 0.5, 0)$, respectively, at 150 K. The solid lines are fitted by Eq. (1). (c) The phonon dispersions along $[2, K, 0]$ of all samples. The solid lines are guides for the eye. (d) The fitted Γ along $[2, K, 0]$. The solid lines are guides for the eye. The dashed line is Γ_{cal} as described in the main text. We note that the data here were all obtained on EIGER with the same configuration, so only one Γ_{cal} is considered. The large Γ value at $(2, 0.6, 0)$ for the $x = 1$ sample is due to the resolution effect [53]. (e) The doping dependence of the Debye temperatures obtained by various methods as described in the main text. Θ_D^H , Θ_D^L , and Θ_D^P are the Debye temperatures calculated based on high-temperature specific heats, low-temperature specific heats, and the phonon velocities, respectively. The dashed lines are guides to the eye. (f) The doping dependence of EPC constant λ_{DFT} and λ_{EXP} obtained by LDA calculations and Eq. (2), respectively. The phonon energy width Γ at $(2, 0.5, 0)$ is also shown. The dashed lines are guides to the eye.

which is due to different crystal structures. The values of Γ of the $x = 1$ sample and that of the $x = 0.65$ sample at 5 K are close to Γ_{cal} for undamped phonons, which is calculated by considering the phonon dispersion and instrument resolution [60] at small Q 's. Therefore, we can consider that there is no or little damping effect for the TA phonons in the $x = 1$ sample and the TA phonons in the $x \leq 0.65$ sample with the triclinic structure.

The evolution of the TA phonons provides a quantitative understanding on the change of the Debye temperature. The Debye temperature Θ_D^H can be obtained by fitting the high-temperature specific heat with the Debye model [53], which is shown in Fig. 3(e). Θ_D^H smoothly

decreases with decreasing x , which is consistent with the lowering of the TA phonon dispersion as shown in Fig. 3(c). On the other hand, a previous report has shown that the Debye temperature Θ_D^L obtained by the low-temperature specific heat drops dramatically around the optimal doping level [29], as shown together with our results in Fig. 3(e) [53]. We note that Θ_D^L is calculated by fitting the low-temperature specific heat C with $\gamma T + \beta T^3$, where $\beta = 12\pi^4 k_B / 5(\Theta_D^L)^3$ according to the low-temperature limit of the Debye model. As Θ_D^L is proportional to the effective sonic velocity ν_{eff} , which can be estimated by the LA and TA phonon velocities (ν_L and ν_T) at low energies as $\nu_{eff}^{-3} = (1/3)\nu_L^{-3} + (2/3)\nu_T^{-3}$ [53]. By considering the broadening of the TA phonons that effectively gives a distribution of ν_T , we can calculate Θ_D^P as shown in Fig. 3(e), which quantitatively explains the drop of Θ_D^L around the optimal doping level.

The large damping of TA phonons typically come from strong EPC. According to BCS theory, the EPC constant λ is related to T_c as the following empirical equation [61]

$$\lambda = \frac{1.04 + \mu^* \ln(\Theta/1.45T_c)}{(1 - 0.62\mu^*) \ln(\Theta/1.45T_c) - 1.04}, \quad (2)$$

where μ^* is the pseudopotential. The value of μ^* may be taken from 0.1 to 0.2. Here we choose μ^* to be 0.16 to compare with the theoretical calculation of λ_{DFT} as discussed later. According to the experimental values of Θ_D^L [Fig. 3(e)] and T_c , the doping dependence of λ_{EXP} is shown in Fig. 3(f). We note that changing μ^* only changes the absolute value of λ_{EXP} and does not change the overall doping dependence. With decrease x from 1 to 0.7, λ_{EXP} quickly increases from about 0.45 to 0.7. We note that such change of λ is quantitatively consistent with the change of Γ at $(2,0.5,0)$, further suggesting the origin of the phonon broadening as from the EPC coupling. For $x \leq 0.65$ where the low-temperature structure becomes triclinic and no damping of TA phonons presents, λ_{EXP} drops below 0.5. This means that the change of T_c in the BSNA system can be readily explained by the increase of EPC and the decrease of the Debye temperature within the mechanism of BCS theory.

To understand the broadening of the TA phonons, we calculated the phonon spectra and EPC by the first-principles calculations. Figures 4(a) and 4(b) show the calculated phonon dispersion weighted by the phonon linewidth for tetragonal SrNi_2As_2 and $\text{Ba}_{0.5}\text{Sr}_{0.5}\text{Ni}_2\text{As}_2$, where the crystal structures are fully relaxed. We also create a triclinic SrNi_2As_2 by changing the Ba into Sr in the structure of triclinic BaNi_2As_2 and fully relax the lattice, whose spectra are shown in Fig. 4(c). It is clear that there is no substantial change for different doping levels and structures. Moreover, the EPC constant λ also shows little doping dependence, as already shown in Fig. 3(f). We note that while the large λ is consistent with the experimental value around the optimal doping level, the calculated broadening of the phonons happens mostly for optical phonons. We thus fix the structure of SrNi_2As_2 by the experimental parameters without relaxation. The

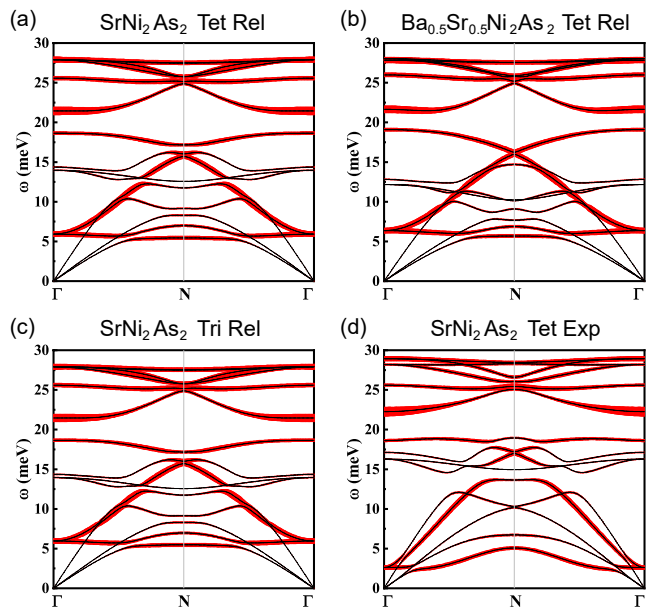


FIG. 4. Phonon dispersions weighted by the phonon linewidth (red circles) for fully relaxed (Rel) (a) tetragonal (Tet) SrNi_2As_2 , (b) tetragonal $\text{Ba}_{0.5}\text{Sr}_{0.5}\text{Ni}_2\text{As}_2$ and (c) triclinic (Tri) SrNi_2As_2 . (d) Phonon dispersions weighted by the phonon linewidth calculated by considering the experimental (Exp) parameters for tetragonal SrNi_2As_2 .

acoustic phonons at lower energies become significantly broader, as shown in Fig. 4(d), suggesting large acoustic-optical phonon hybridization in real materials. We note that the value of λ remains unchanged even when using the experimental lattice parameters.

Our results on the large damping of TA phonons cannot be explained by nematic fluctuations. Previous measurements on iron-based superconductors have shown that the TA phonons become slightly softened at low energies and small q near Bragg peaks in the presence of nematic fluctuations [62–64] as shown in Fig. 1(b), because nematic fluctuations are long wavelength. Moreover, such softening should be reduced with increasing temperature due to the decrease of nematic susceptibility [62–64]. However, our results show that the TA phonons in the optimally doped samples are significantly damped over the whole Q range with little temperature dependence, which clearly cannot be understood within the picture based on nematic fluctuations. It should be noted that even the presence of nematic fluctuations in nickel pnictides may be in doubt [65].

The large damping effects cannot come from CDW fluctuations either. Phonon softening and damping effects have been widely observed in many CDW systems [66–70] and BaNi_2As_2 [71, 72]. However, we note that such softening and damping of phonons are confined around the CDW wave vectors as shown in Fig. 1(b) and have strong temperature dependence associated with the CDW order. In our case, the damping of TA phonons is found over the whole Q and temperature ranges in the

optimally doped samples where no CDW order occurs.

We attribute the large damping effects of TA phonons to the large EPC and acoustic-optical phonon hybridization in this system. As shown above, theoretical calculations have revealed strong electron phonon couplings and large phonon linewidths of many optical phonons. Indeed, the linewidth of the lowest optical branch around 6 meV (Fig. 4), i.e. the E_g mode in Raman scattering, is already very large at room temperature in BaNi_2As_2 [42]. The FWHM of the E_g mode is about 2.7 meV, close to the values of our results at large K 's. The TA phonons are thus broadened through the acoustic-optical phonon hybridization. It has been shown in some thermoelectric materials that strong acoustic-optical hybridization can lead to low lattice thermal conductivity κ_{lat} [73, 74]. In our samples, we have found that κ_{lat} in the optimally doped samples is indeed strongly suppressed [75], consistent with the large acoustic-optical phonon hybridization.

The large EPC naturally explains the superconductivity of the BSNA system within the conventional BCS framework. As shown by the above calculations and previous studies [34], the EPC constant λ is supposed to be about 0.7 without introducing strong electron-electron correlations. We note that recent studies have shown the weak nature of correlations in BSNA [38], suggesting the reliability of our calculations. Such large λ naturally gives a T_c higher than 3 K according to the McMillan equation [61]. Therefore, the superconductivity and phonon spectra around optimal doping are very conventional without the need to invoke quantum fluctuations of either CDW or nematicity. This is contrary to the wisdom that the optimal superconductivity in this system may come from an undoped compound and the quantum fluctuations associated with the suppression of the order in this parent compound [29, 38]. Instead, the change of superconductivity with doping should be understood as the sixfold suppression of the superconductivity in un-

doped compounds due to the weakening of the EPC. For BaNi_2As_2 , the decrease of EPC can be easily attributed to the CDW as the change of lattice structure has little effects on the EPC. On the other hand, it is unclear what mechanism results in the suppression of EPC in SrNi_2As_2 , which show no signs of CDW or other order.

IV. CONCLUSIONS

In conclusion, we have shown large damping effects of TA phonons in BSNA, which comes from large EPC and can well reproduce the optimal superconductivity within the conventional framework of the BCS theory. Neither nematicity nor CDW is necessary to be introduced in this mechanism. Our results suggest that the superconductivity in this system should not be understood as the sixfold enhancement from parent compounds but rather is sixfold suppressed in them. The origin of the large EPC and its suppression in SrNi_2As_2 need to be further studied.

ACKNOWLEDGMENTS

S. L. thanks Prof. Pengcheng Dai for discussions. This work is supported by the National Key Research and Development Program of China (Grants No. 2022YFA1403400, No. 2021YFA1400400, No. 2021YFA1400020, No. 2023YFA1406100, No. 2018YFA0704200, and No. 2023YFA1406500), the National Natural Science Foundation of China (Grants No. 12025407, No. 12004426, and No. 12304185), the Chinese Academy of Sciences (Grants No. XDB33000000, No. GJTD-2020-01, No. CAS-WX2023SF-0101, and No. ZDBS-LY-SLH007).

L.S. and J.S. contributed equally to this work.

-
- [1] M. A. Metlitski, D. F. Mross, S. Sachdev, and T. Senthil, Cooper pairing in non-Fermi liquids, *Phys. Rev. B* **91**, 115111 (2015).
 - [2] S. Lederer, Y. Schattner, E. Berg, and S. A. Kivelson, Enhancement of superconductivity near a nematic quantum critical point, *Phys. Rev. Lett.* **114**, 097001 (2015).
 - [3] S. Lederer, Y. Schattner, E. Berg, and S. A. Kivelson, Superconductivity and non-Fermi liquid behavior near a nematic quantum critical point, *Proc. Natl. Acad. Sci. USA* **114**, 4905 (2017).
 - [4] A. Klein, Y. Wu, and A. Chubukov, Multiple intertwined pairing states and temperature-sensitive gap anisotropy for superconductivity at a nematic quantum-critical point, *npj Quantum Mater.* **4**, 55 (2019).
 - [5] R. M. Fernandes, P. P. Orth, and J. Schmalian, Intertwined vestigial order in quantum materials: Nematicity and beyond, *Annu. Rev. Condens. Matter Phys.* **10**, 133 (2019).
 - [6] R. M. Fernandes, A. V. Chubukov, and J. Schmalian, What drives nematic order in iron-based superconductors?, *Nat. Phys.* **10**, 97 (2014).
 - [7] J.-H. Chu, H.-H. Kuo, J. G. Analytis, and I. R. Fisher, Divergent nematic susceptibility in an iron arsenide superconductor, *Science* **337**, 710 (2012).
 - [8] Y. Gallais, R. M. Fernandes, I. Paul, L. Chauvière, Y.-X. Yang, M.-A. Méasson, M. Cazayous, A. Sacuto, D. Colson, and A. Forget, Observation of incipient charge nematicity in $\text{Ba}(\text{Fe}_{1-x}\text{Co}_x)_2\text{As}_2$, *Phys. Rev. Lett.* **111**, 267001 (2013).
 - [9] A. E. Böhmer, P. Burger, F. Hardy, T. Wolf, P. Schweiss, R. Fromknecht, M. Reinecker, W. Schranz, and C. Meingast, Nematic susceptibility of hole-doped and electron-doped baf_2as_2 iron-based superconductors from shear modulus measurements, *Phys. Rev. Lett.* **112**, 047001 (2014).
 - [10] H.-H. Kuo, J.-H. Chu, J. C. Palmstrom, S. A. Kivelson, and I. R. Fisher, Ubiquitous signatures of nematic quantum criticality in optimally doped Fe-based super-

- conductors, *Science* **352**, 958 (2016).
- [11] Z. Liu, Y. Gu, W. Zhang, D. Gong, W. Zhang, T. Xie, X. Lu, X. Ma, X. Zhang, R. Zhang, J. Zhu, C. Ren, L. Shan, X. Qiu, P. Dai, Y.-f. Yang, H. Luo, and S. Li, Nematic quantum critical fluctuations in $\text{BaFe}_{2-x}\text{Ni}_x\text{As}_2$, *Phys. Rev. Lett.* **117**, 157002 (2016).
- [12] Y. Gu, Z. Liu, T. Xie, W. Zhang, D. Gong, D. Hu, X. Ma, C. Li, L. Zhao, L. Lin, Z. Xu, G. Tan, G. Chen, Z. Y. Meng, Y.-f. Yang, H. Luo, and S. Li, Unified phase diagram for iron-based superconductors, *Phys. Rev. Lett.* **119**, 157001 (2017).
- [13] M. Vojta, Lattice symmetry breaking in cuprate superconductors: stripes, nematics, and superconductivity, *Adv. Phys.* **58**, 699 (2009).
- [14] V. Hinkov, D. Haug, B. Fauqué, P. Bourges, Y. Sidis, A. Ivanov, C. Bernhard, C. T. Lin, and B. Keimer, Electronic liquid crystal state in the high-temperature superconductor $\text{YBa}_2\text{Cu}_3\text{O}_{6.45}$, *Science* **319**, 597 (2008).
- [15] R. Daou, J. Chang, D. LeBoeuf, O. Cyr-Choinière, F. Laliberté, N. Doiron-Leyraud, B. Ramshaw, R. Liang, D. Bonn, W. Hardy, *et al.*, Broken rotational symmetry in the pseudogap phase of a high- T_c superconductor, *Nature* **463**, 519 (2010).
- [16] Y. Sato, S. Kasahara, H. Murayama, Y. Kasahara, E.-G. Moon, T. Nishizaki, T. Loew, J. Porras, B. Keimer, T. Shibauchi, and Y. Matsuda, Thermodynamic evidence for a nematic phase transition at the onset of the pseudogap in $\text{YBa}_2\text{Cu}_3\text{O}_y$, *Nat. Phys.* **13**, 1074 (2017).
- [17] H. Murayama, Y. Sato, R. Kurihara, S. Kasahara, Y. Mizukami, Y. Kasahara, H. Uchiyama, A. Yamamoto, E.-G. Moon, J. Cai, J. Freyermuth, M. Greven, T. Shibauchi, and Y. Matsuda, Diagonal nematicity in the pseudogap phase of $\text{HgBa}_2\text{CuO}_{4+\delta}$, *Nat. Commun.* **10**, 3282 (2019).
- [18] N. Auvray, B. Loret, S. Benhabib, M. Cazayous, R. Zhong, J. Schneeloch, G. Gu, A. Forget, D. Colson, I. Paul, *et al.*, Nematic fluctuations in the cuprate superconductor $\text{Bi}_2\text{Sr}_2\text{CaCu}_2\text{O}_{8+\delta}$, *Nat. Commun.* **10**, 5209 (2019).
- [19] K. Ishida, S. Hosoi, Y. Teramoto, T. Usui, Y. Mizukami, K. Itaka, Y. Matsuda, T. Watanabe, and T. Shibauchi, Divergent nematic susceptibility near the pseudogap critical point in a cuprate superconductor, *J. Phys. Soc. Jpn.* **89**, 064707 (2020).
- [20] S. Hosoi, K. Matsuura, K. Ishida, H. Wang, Y. Mizukami, T. Watashige, S. Kasahara, Y. Matsuda, and T. Shibauchi, Nematic quantum critical point without magnetism in $\text{FeSe}_{1-x}\text{S}_{1-x}$ superconductor, *Proc. Natl Acad. Sci. USA* **113**, 8139 (2016).
- [21] O. Cyr-Choinière, G. Grissonnanche, S. Badoux, J. Day, D. A. Bonn, W. N. Hardy, R. Liang, N. Doiron-Leyraud, and L. Taillefer, Two types of nematicity in the phase diagram of the cuprate superconductor $\text{YBa}_2\text{Cu}_3\text{O}_y$, *Phys. Rev. B* **92**, 224502 (2015).
- [22] O. Cyr-Choinière, R. Daou, F. Laliberté, C. Collignon, S. Badoux, D. LeBoeuf, J. Chang, B. J. Ramshaw, D. A. Bonn, W. N. Hardy, R. Liang, J.-Q. Yan, J.-G. Cheng, J.-S. Zhou, J. B. Goodenough, S. Pyon, T. Takayama, H. Takagi, N. Doiron-Leyraud, and L. Taillefer, Pseudogap temperature T^* of cuprate superconductors from the Nernst effect, *Phys. Rev. B* **97**, 064502 (2018).
- [23] T. Xie, Z. Liu, Y. Gu, D. Gong, H. Mao, J. Liu, C. Hu, X. Ma, Y. Yao, L. Zhao, X. Zhou, J. Schneeloch, G. Gu, S. Danilkin, Y. feng Yang, H. Luo, and S. Li, Tracking the nematicity in cuprate superconductors: a resistivity study under uniaxial pressure, *J. Phys.: Condens. Matter* **34**, 334001 (2022).
- [24] J. C. S. Davis and D.-H. Lee, Concepts relating magnetic interactions, intertwined electronic orders, and strongly correlated superconductivity, *Proc. Natl. Acad. Sci. USA* **110**, 17623 (2013).
- [25] E. Fradkin, S. A. Kivelson, and J. M. Tranquada, Colloquium: Theory of intertwined orders in high temperature superconductors, *Rev. Mod. Phys.* **87**, 457 (2015).
- [26] S. A. Kivelson, E. Fradkin, and V. J. Emery, Electronic liquid-crystal phases of a doped Mott insulator, *Nature* **393**, 550 (1998).
- [27] P. A. Lee, N. Nagaosa, and X.-G. Wen, Doping a Mott insulator: Physics of high-temperature superconductivity, *Rev. Mod. Phys.* **78**, 17 (2006).
- [28] P. Dai, Antiferromagnetic order and spin dynamics in iron-based superconductors, *Rev. Mod. Phys.* **87**, 855 (2015).
- [29] C. Eckberg, D. J. Campbell, T. Metz, J. Collini, H. Hodovanets, T. Drye, P. Zavalij, M. H. Christensen, R. M. Fernandes, S. Lee, P. Abbamonte, J. W. Lynn, and J. Paglione, Sixfold enhancement of superconductivity in a tunable electronic nematic system, *Nat. Phys.* **16**, 346 (2020).
- [30] F. Ronning, N. Kurita, E. D. Bauer, B. L. Scott, T. Park, T. Klimczuk, R. Movshovich, and J. D. Thompson, The first order phase transition and superconductivity in BaNi_2As_2 single crystals, *J. Phys.:Condens. Matter* **20**, 342203 (2008).
- [31] A. S. Sefat, M. A. McGuire, R. Jin, B. C. Sales, D. Mandrus, F. Ronning, E. D. Bauer, and Y. Mozharivskiy, Structure and anisotropic properties of $\text{BaFe}_{2-x}\text{Ni}_x\text{As}_2$ ($x = 0, 1$, and 2) single crystals, *Phys. Rev. B* **79**, 094508 (2009).
- [32] E. D. Bauer, F. Ronning, B. L. Scott, and J. D. Thompson, Superconductivity in SrNi_2As_2 single crystals, *Phys. Rev. B* **78**, 172504 (2008).
- [33] K. Kothapalli, F. Ronning, E. D. Bauer, A. J. Schultz, and H. Nakotte, Single-crystal neutron diffraction studies on Ni-based metal-pnictide superconductor BaNi_2As_2 , *J. Phys. Conf. Ser.* **251**, 012010 (2010).
- [34] A. Subedi and D. J. Singh, Density functional study of BaNi_2As_2 : Electronic structure, phonons, and electron-phonon superconductivity, *Phys. Rev. B* **78**, 132511 (2008).
- [35] K. Kudo, M. Takasuga, Y. Okamoto, Z. Hiroi, and M. Nohara, Giant Phonon Softening and Enhancement of Superconductivity by Phosphorus Doping of BaNi_2As_2 , *Phys. Rev. Lett.* **109**, 097002 (2012).
- [36] K. Kudo, M. Takasuga, and M. Nohara, Copper doping of BaNi_2As_2 : Giant phonon softening and superconductivity enhancement (2017), arXiv:1704.04854.
- [37] C. Eckberg, L. Wang, H. Hodovanets, H. Kim, D. J. Campbell, P. Zavalij, P. Piccoli, and J. Paglione, Evolution of structure and superconductivity in $\text{Ba}(\text{Ni}_{1-x}\text{Co}_x)_2\text{As}_2$, *Phys. Rev. B* **97**, 224505 (2018).
- [38] D. M. Narayan, P. Hao, R. Kurlito, B. S. Berggren, A. G. Linn, C. Eckberg, P. Saraf, J. Collini, P. Zavalij, M. Hashimoto, D. Lu, R. M. Fernandes, J. Paglione, and D. S. Dessau, Potential Lifshitz transition at optimal substitution in nematic pnictide $\text{Ba}_{1-x}\text{Sr}_x\text{Ni}_2\text{As}_2$, *Sci. Adv.* **9**, eadi4966 (2023).
- [39] D. Hirai, F. von Rohr, and R. J. Cava, Emergence of

- superconductivity in $\text{BaNi}_2(\text{Ge}_{1-x}\text{P}_x)_2$ at a structural instability, *Phys. Rev. B* **86**, 100505 (2012).
- [40] V. Hlukhyy, A. V. Hoffmann, V. Grinenko, J. Scheiter, F. Hummel, D. Johrendt, and T. F. Fässler, Structural instability and superconductivity in the solid solution $\text{SrNi}_2(\text{P}_{1-x}\text{Ge}_x)_2$, *Phys. Status Solidi B* **254**, 1600351 (2017).
- [41] M. Merz, L. Wang, T. Wolf, P. Nagel, C. Meingast, and S. Schuppler, Rotational symmetry breaking at the incommensurate charge-density-wave transition in $\text{Ba}(\text{Ni}, \text{Co})_2(\text{As}, \text{P})_2$: Possible nematic phase induced by charge/orbital fluctuations, *Phys. Rev. B* **104**, 184509 (2021).
- [42] Y. Yao, R. Willa, T. Lacmann, S.-M. Souliou, M. Frachet, K. Willa, M. Merz, F. Weber, C. Meingast, R. Heid, A.-A. Haghighirad, J. Schmalian, and M. L. Tacon, An electronic nematic liquid in BaNi_2As_2 , *Nat. Commun.* **13**, 4535 (2022).
- [43] S. Lee, G. de la Peña, S. X.-L. Sun, M. Mitrano, Y. Fang, H. Jang, J.-S. Lee, C. Eckberg, D. Campbell, J. Collini, J. Paglione, F. M. F. de Groot, and P. Abbamonte, Unconventional charge density wave order in the pnictide superconductor $\text{Ba}(\text{Ni}_{1-x}\text{Co}_x)_2\text{As}_2$, *Phys. Rev. Lett.* **122**, 147601 (2019).
- [44] S. Lee, J. Collini, S. X.-L. Sun, M. Mitrano, X. Guo, C. Eckberg, J. Paglione, E. Fradkin, and P. Abbamonte, Multiple charge density waves and superconductivity nucleation at antiphase domain walls in the nematic pnictide $\text{Ba}_{1-x}\text{Sr}_x\text{Ni}_2\text{As}_2$, *Phys. Rev. Lett.* **127**, 027602 (2021).
- [45] E. Morosan, H. W. Zandbergen, B. S. Dennis, J. W. G. Bos, Y. Onose, T. Klimczuk, A. P. Ramirez, and N. P. O. R. J. Cava, Superconductivity in Cu_xTiSe_2 , *Nat. Phys.* **2**, 544 (2006).
- [46] B. Sipos, A. F. Kusmartseva, A. Akrap, H. Berger, L. Forró, and E. Tutiš, From Mott state to superconductivity in 1T-TaS_2 , *Nat. Mater.* **7**, 960 (2008).
- [47] K. E. Wagner, E. Morosan, Y. S. Hor, J. Tao, Y. Zhu, T. Sanders, T. M. McQueen, H. W. Zandbergen, A. J. Williams, D. V. West, and R. J. Cava, Tuning the charge density wave and superconductivity in Cu_xTaS_2 , *Phys. Rev. B* **78**, 104520 (2008).
- [48] E. Morosan, K. E. Wagner, L. L. Zhao, Y. Hor, A. J. Williams, J. Tao, Y. Zhu, and R. J. Cava, Multiple electronic transitions and superconductivity in Pd_xTiSe_2 , *Phys. Rev. B* **81**, 094524 (2010).
- [49] Y. Liu, D. F. Shao, L. J. Li, W. J. Lu, X. D. Zhu, P. Tong, R. C. Xiao, L. S. Ling, C. Y. Xi, L. Pi, H. F. Tian, H. X. Yang, J. Q. Li, W. H. Song, X. B. Zhu, and Y. P. Sun, Nature of charge density waves and superconductivity in $1\text{T} - \text{TaSe}_{2-x}\text{Te}_x$, *Phys. Rev. B* **94**, 045131 (2016).
- [50] C. Meingast, A. Shukla, L. Wang, R. Heid, F. Hardy, M. Frachet, K. Willa, T. Lacmann, M. Le Tacon, M. Merz, A.-A. Haghighirad, and T. Wolf, Charge density wave transitions, soft phonon, and possible electronic nematicity in $\text{BaNi}_2(\text{As}_{1-x}\text{P}_x)_2$, *Phys. Rev. B* **106**, 144507 (2022).
- [51] U. Stuhr, B. Roessli, S. Gvasaliya, H. M. Rønnow, U. Filges, D. Graf, A. Bollhalder, D. Hohl, R. Bürge, M. Schild, L. Holitzner, C. Kaegi, P. Keller, and T. Mühlebach, The thermal triple-axis-spectrometer EIGER at the continuous spallation source SINQ, *Nucl. Instrum. Methods Phys. Res., Sect. A* **A853**, 16 (2017).
- [52] S. A. Danilkin, G. Horton, R. Moore, G. Braoudakis, and M. E. Hagen, The TAIPAN thermal triple-axis spectrometer at the OPAL reactor, *J. Neutron Res.* **15**, 55 (2007).
- [53] See supplementary materials for sample information and additional data for the longitudinal and transverse acoustic phonons, and specific heats.
- [54] E. Farhi, Y. Debab, and P. Willendrup, iFit: A new data analysis framework. Applications for data reduction and optimization of neutron scattering instrument simulations with McStas, *J. Neut. Res.* **17**, 5 (2013).
- [55] P. Giannozzi, S. Baroni, N. Bonini, M. Calandra, R. Car, C. Cavazzoni, D. Ceresoli, G. L. Chiarotti, M. Cococcioni, I. Dabo, A. D. Corso, S. de Gironcoli, S. Fabris, G. Fratesi, R. Gebauer, U. Gerstmann, C. Gougoussis, A. Kokalj, M. Lazzeri, L. Martin-Samos, N. Marzari, F. Mauri, R. Mazzarello, S. Paolini, A. Pasquarello, L. Paulatto, C. Sbraccia, S. Scandolo, G. Scalauzero, A. P. Seitsonen, A. Smogunov, P. Umari, and R. M. Wentzcovitch, Quantum espresso: a modular and open-source software project for quantum simulations of materials, *J. Phys.: Condens. Matter* **21**, 395502 (2009).
- [56] L. Bellaïche and D. Vanderbilt, Virtual crystal approximation revisited: Application to dielectric and piezoelectric properties of perovskites, *Phys. Rev. B* **61**, 7877 (2000).
- [57] J. P. Perdew, K. Burke, and M. Ernzerhof, Generalized gradient approximation made simple, *Phys. Rev. Lett.* **77**, 3865 (1996).
- [58] S. Baroni, S. de Gironcoli, A. Dal Corso, and P. Giannozzi, Phonons and related crystal properties from density-functional perturbation theory, *Rev. Mod. Phys.* **73**, 515 (2001).
- [59] G. Shirane, S. M. Shapiro, and J. M. Tranquada, *Neutron scattering with a triple-axis spectrometer* (Cambridge University Press, 2002).
- [60] N. J. Chesser and J. D. Axe, Derivation and experimental verification of the normalized resolution function for inelastic neutron scattering, *Acta Cryst.* **A29**, 160 (1973).
- [61] W. L. McMillan, Transition temperature of strongly-coupled superconductors, *Phys. Rev.* **167**, 331 (1968).
- [62] F. Weber, D. Parshall, L. Pintschovius, J.-P. Castellan, M. Kauth, M. Merz, T. Wolf, M. Schütt, J. Schmalian, R. M. Fernandes, and D. Reznik, Soft phonons reveal the nematic correlation length in $\text{Ba}(\text{Fe}_{0.94}\text{Co}_{0.06})_2\text{As}_2$, *Phys. Rev. B* **98**, 014516 (2018).
- [63] Y. Li, Z. Yamani, Y. Song, W. Wang, C. Zhang, D. W. Tam, T. Chen, D. Hu, Z. Xu, S. Chi, K. Xia, L. Zhang, S. Cui, W. Guo, Z. Fang, Y. Liu, and P. Dai, Dynamic spin-lattice coupling and nematic fluctuations in NaFeAs , *Phys. Rev. X* **8**, 021056 (2018).
- [64] A. M. Merritt, F. Weber, J.-P. Castellan, T. Wolf, D. Ishikawa, A. H. Said, A. Alatas, R. M. Fernandes, A. Q. R. Baron, and D. Reznik, Nematic correlation length in iron-based superconductors probed by inelastic x-ray scattering, *Phys. Rev. Lett.* **124**, 157001 (2020).
- [65] M. Frachet, P. W. Wiecki, T. Lacmann, S. M. Souliou, K. Willa, C. Meingast, M. Merz, A.-A. Haghighirad, M. L. Tacon, and A. E. Böhrer, Elastoresistivity in the incommensurate charge density wave phase of $\text{BaNi}_2(\text{As}_{1-x}\text{P}_x)_2$, *npj Quantum Mater.* **7**, 115 (2022).
- [66] K. Carneiro, G. Shirane, S. A. Werner, and S. Kaiser, Lattice dynamics of $\text{K}_2\text{Pt}(\text{CN})_4\text{Br}_{0.3}\cdot 3.2\text{D}_2\text{O}$ (KCP) studied by inelastic neutron scattering, *Phys. Rev. B* **13**, 4258 (1976).

- [67] F. Weber, S. Rosenkranz, J.-P. Castellan, R. Osborn, R. Hott, R. Heid, K.-P. Bohnen, T. Egami, A. H. Said, and D. Reznik, Extended phonon collapse and the origin of the charge-density wave in $2H\text{-NbSe}_2$, *Phys. Rev. Lett.* **107**, 107403 (2011).
- [68] P. Monceau, Electronic crystals: an experimental review, *Adv. Phys.* **61**, 325 (2012).
- [69] E. Blackburn, J. Chang, A. H. Said, B. M. Leu, R. Liang, D. A. Bonn, W. N. Hardy, E. M. Forgan, and S. M. Hayden, Inelastic x-ray study of phonon broadening and charge-density wave formation in ortho-ii-ordered $\text{YBa}_2\text{Cu}_3\text{O}_{6.54}$, *Phys. Rev. B* **88**, 054506 (2013).
- [70] H. Miao, D. Ishikawa, R. Heid, M. Le Tacon, G. Fabbri, D. Meyers, G. D. Gu, A. Q. R. Baron, and M. P. M. Dean, Incommensurate phonon anomaly and the nature of charge density waves in cuprates, *Phys. Rev. X* **8**, 011008 (2018).
- [71] S. M. Souliou, T. Lacmann, R. Heid, C. Meingast, M. Frachet, L. Paolasini, A.-A. Haghighirad, M. Merz, A. Bosak, and M. Le Tacon, Soft-phonon and charge-density-wave formation in nematic BaNi_2As_2 , *Phys. Rev. Lett.* **129**, 247602 (2022).
- [72] Y. Song, S. Wu, X. Chen, Y. He, H. Uchiyama, B. Li, S. Cao, J. Guo, G. Cao, and R. Birgeneau, Phonon softening and slowing-down of charge density wave fluctuations in BaNi_2As_2 , *Phys. Rev. B* **107**, L041113 (2023).
- [73] W. Li, J. Carrete, G. K. H. Madsen, and N. Mingo, Influence of the optical-acoustic phonon hybridization on phonon scattering and thermal conductivity, *Phys. Rev. B* **93**, 205203 (2016).
- [74] F.-X. Bai, H. Yu, D. Peng, H.-J. Pang, L. Yu, L.-C. Chen, J. Mao, Q. Zhang, and X.-J. Chen, Strong acoustic-optical phonon coupling in high-performance thermoelectric material $\text{Bi}_{0.5}\text{Sb}_{1.5}\text{Te}_3$, *Mater. Today Phys.* **37**, 101200 (2023).
- [75] X. Wu, L. Song, H. Zhao, and S. Li, Unpublished.